Journal of Dynamic Disasters 2 (2026) 100057

Contents lists available at ScienceDirect

Journal of Dynamic Disasters

journal homepage: http://www.keaipublishing.com/en/journals/journal of dynamic disasters/

Case Study

Estimation of the damping ratio using high sampling rate GPS and RTS measurements ☆

Marco Gatti

University of Ferrara - Department of Engineering, Via Saragat 1, 44123 Ferrara, Italy

ARTICLE INFO

Keywords:
Damping ratio
GPS
RTS
Building
Tie

ABSTRACT

"High sampling rate" GPS/GNSS (Global Positioning System/Global Navigation Satellite System) and RTS (Robotic Total Station) measurements were used to extract the vibration functions of, respectively, ca. thirty buildings hosting permanent GPS stations and the ties of four masonry arches of a church.
The logarithmic decrement, frequency response, frequency domain decomposition and spectral response methods were applied to the measurements to estimate the damping ratio ζ.
The methods' costs, times, calculation codes and application to the case studies were compared to evaluate whether "high sampling rate" GPS and RTS are suitable for estimation of the damping ratio ζ of a building or a tie.

Introduction

Structural dynamics requires knowledge of the elastic period of vibration T_o and the damping ratio ζ (Crandall, 1970). Estimation of T_o is unique and immediate. For that of ζ, various investigative models have been proposed since 1973, on the assumption of viscous or non-viscous, linear or non-linear dampings (Adhikari, 2013; Bert, 1973; Fang et al., 1999; Liu et al., 2000; Maia et al, 1998; Maximov et al, 2021; Meirovitch, 1997; Minas and Inman, 1991; Nakić, 2013; Prells and Friswell, 2000; Truhar et al., 2017; Vasques et al., 2010a, 2010b; Veselić, 2011; Woodhouse, 1998). Corresponding to such models are many simulated or experimental methods (Andrianne and Dimitriadis, 2012; Beards, 1996; Béliveau, 1976; Chen et al., 1996; Dalenbring, 1999; Deniβen et al., 2014; Ding and Law, 2011; Fabunmi et al., 1988; Jakovčević Stor et al., 2022; Jeary, 1986; Li and Law, 2009; Min et al., 2012; Phani and Woodhouse, 2007, 2009; Pradhan and Modak, 2012; Prandina et al., 2009; Segalman, 1987; Sivaprasad et al., 2009; Truhar and Petrač, 2022; Truhar et al., 2015; Vinokur, 2003). The experimental methods have almost always required a priori knowledge of the vibrations, induced by excitations and classically measured with accelerometer sensors.

In dynamic structural monitoring applications, high sampling rate geodetic and topographic sensors have been available for some years now, such as GPS/GNSS (Global Positioning System/Global Navigation Satellite System) receivers or RTS (Robotic Total Stations) (Breuer et al., 2015; Brownjohn et al., 2012; Bürki et al., 2011; Charalampous et al., 2015; Cosser et al., 2003; Ehrhart and Lienhart, 2016; Ehrhart et al., 2016; Gatti, 2022; Li et al., 2004; Moschas and Stiros, 2013 and 2014; Psimoulis and Stiros, 2012 and 2013; Psimoulis et al., 2016; Radovanovic and Teskey, 2001; Stache and Zimmer, 2007; Venuti and Bruno, 2008; Yoshida et al., 2002; Yu et al., 2017). Compared to accelerometers, they have the advantage of measuring the vibrations in displacement.

Therefore, it seemed interesting to investigate their use by calculating the vibration functions of a structure based on their measurements and then to estimate the damping ratio ζ by means of some of the most classic methods proposed in the literature. In particular, the vibration measurements of ca. thirty buildings hosting permanent GPS stations and of the ties of four masonry arches

☆ Peer review under responsibility of KeAi Communications Co., Ltd.

E-mail address: marco.gatti@unife.it

https://doi.org/10.1016/j.jdd.2026.100057
Received 30 October 2025; Received in revised form 14 February 2026; Accepted 17 March 2026
2950-5763/© 2026 The Author(s). Published by Elsevier B.V. on behalf of KeAi Communications Co., Ltd. This is an open access article under the CC BY license (http://creativecommons.org/licenses/by/4.0/)

measured with a RTS were available. The damping ratios ζ were estimated by application to the corresponding functions of the logarithmic decrement, frequency response, frequency domain decomposition and spectral response methods (Bachmann et al., 1995; Blandon and Priestley, 2005; Brincker et al., 2000, 2001; Chopra, 1995; Muravyov, 1998; Clough and Penzien, 1993; Ewins, 1984; Gatti, 2018; Muscia, 1991; Paz and Saunders, 1985).

The study assessed the potential of "high sampling rate" GPS and RTS measurements to determine the vibration functions in terms of continuous recording, sampling intervals and amplitudes. Moreover, the methods' costs, times, calculation codes and application to the case studies were compared to evaluate the suitability of such measurements for estimation of the damping ratio ζ.

The estimated damping ratio ζ values were practically identical for the various methods and numerically similar to those reported in the scientific literature (Elnashai and Di Sarno, 2008; Lin et al., 2005; Rao, 2011; Satake et al., 2003). The frequency domain decomposition and spectral response methods, while being more laborious and computationally costly, can be applied perfectly to these measurements, unlike the logarithmic decrement method even though it is simpler and less costly in computational terms.

All in all, while taking into account the measurement constraints typical of GPS/GNSS and RTS measurements and the fact that not all estimation methods are by definition applicable to them, the study has still allowed us to evaluate their potential in the "high frequency" range in terms of continuous recording, sampling intervals and amplitudes as well as the parameters that influence estimation of the damping ratio ζ in terms of costs, times, calculation codes and application in real conditions.

Finally, the so-called "high sampling rate" of these methods is still a limitation that prevents full use in the field of structural dynamics.

1. Description of the investigated methods

The logarithmic decrement method, the frequency response method (Ewins, 1984), the frequency domain decomposition method (Brincker et al., 2000, 2001) and the spectral analysis method (Gatti, 2018) were considered for estimation of ζ.

1.1. Logarithmic decrement

Logarithmic decrement δ is represented by the reduction in amplitude, for successive cycles, of the vibration function x(t):

$$\delta = \ln \frac{x(t)}{x(t, To)} \tag{1}$$

or expressed over a number of entire cycles n:

$$\delta = \frac{1}{n} \ln \frac{x_i}{x_{i+n}} \tag{2}$$

The solution of ζ is contained in the following formula:

$$\zeta = \frac{\delta}{\sqrt{\delta^2 + 4\pi^2}} \tag{3}$$

equivalent to $\zeta = \frac{\delta}{2\pi}$ for values ≤ 0.3.

The approximation with which ζ is estimated depends on the temporal resolution of the vibration function, that is, being in discrete form, on the sampling rate.

1.2. Frequency response

The frequency response function FRF is the ratio of the Fourier transforms FFT $\tilde{x}$ and $\tilde{f}$ of the vibration functions of the response x(t) to the external force f(t):

$$FRF = \frac{\tilde{x}}{\tilde{f}} \tag{4}$$

The ratio can be expressed in numerical form only if the two functions are discretized at the same rate δt or at rates that are multiples of δt. To solve the damping ratio ζ, one can use the bandwidth method (Chopra, 1995):

$$\zeta = \frac{\omega_{f2}^2 - \omega_{f1}^2}{4\omega_o} \tag{5}$$

approximable to:

$$\zeta = \frac{\omega_{f2} - \omega_{f1}}{2\omega_o} \tag{6}$$

where ω_0 is the pulsation for the first mode frequency f_o while the pulsations ω_{f2} and ω_{f1} are calculated on the FRF diagram (Fig. 1) in correspondence of the ordinate $A_{max}/\sqrt{2}$.

The approximation by which ζ is estimated depends on the frequency resolution related, as is well known (Géradin and Rixen, 1997), to the sampling rate and the sampling number.

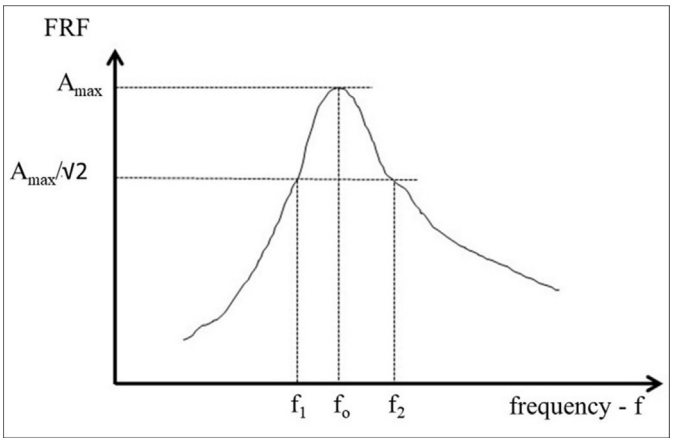


Fig. 1. Diagram of the frequency response function (FRF).

1.3. Frequency domain decomposition

Frequency domain decomposition (FDD) is the decomposition, in the frequency domain, of the vibration function x(t) in N modal contributions at a single degree of freedom (SDOF) via a power spectral density (PSD). The PSD S(ω) matrix is estimated from the measured responses and, for each frequency line, is subjected to a singular value decomposition:

$$S(\omega) = U(\omega)\Sigma(\omega)U^T(\omega) \tag{7}$$

where $\Sigma(\omega)$ contains the singular values and U(ω) the corresponding singular vectors.

The peaks of the first singular value allow us to identify the system's natural frequencies; once the single mode has been isolated by selecting the frequency band of interest, the associated modal response is transformed back into the time domain using an inverse Fourier transform (IFFT), obtaining the modal impulse response h(t). The reconstructed h(t) function is assumed as the signal to which the logarithmic decrement method introduced in Section 1, §1.1 is applied to derive the damping ratio ζ.

Similarly to the previous method, the accuracy with which ζ is estimated depends on the frequency resolution of the inverse FFT.

A method conceptually similar in the frequency domain was proposed by Hermans et al. (1998) in the context of a maximum likelihood (ML)-type formulation.

1.4. Spectral analysis

Full spectral analysis consists in determination of the spectrograms F(T) and X(T), i.e. the anti-Fourier transforms (AFT) of the external force f(t) and the response x(t).

In general, a spectrogram is the ratio between the FFT of a discrete function and its transfer function $H(T,\zeta)$, which depends on the period T and the damping ratio ζ, for which, starting from the definition of the spectrogram of the response x(t) and the external force f(t), we have:

$$\mathrm{X(T)} = \frac{\tilde{\mathrm{x}}}{\mathrm{H(T},\zeta)} \tag{8}$$

$$\mathrm{F(T)} = \frac{\tilde{\mathrm{f}}}{\mathrm{H(T},\zeta)} \tag{9}$$

or rather:

$$\mathrm{H(T},\zeta) = \frac{\tilde{\mathrm{f}}}{\mathrm{F(T)}} = \frac{\tilde{\mathrm{x}}}{\mathrm{X(T)}} \tag{10}$$

$$\mathrm{H(T},\zeta) = \frac{\mathrm{F(T)}}{\mathrm{X(T)}} = \frac{\tilde{\mathrm{f}}}{\tilde{\mathrm{x}}} = \frac{1}{\mathrm{FRF}} \tag{11}$$

The spectral analysis is similar to the FRF with one substantial difference: the possibility to obtain the AFT without the sampling rate of the vibration functions being identical or a multiple.

The solution of the damping ratio ζ is obtained, when the value of the first mode period T_o is known, in correspondence of the value of ζ that minimizes the transfer function:

$$\zeta = \min \mathrm{H}\left(\mathrm{T_o},\zeta\right) \tag{12}$$

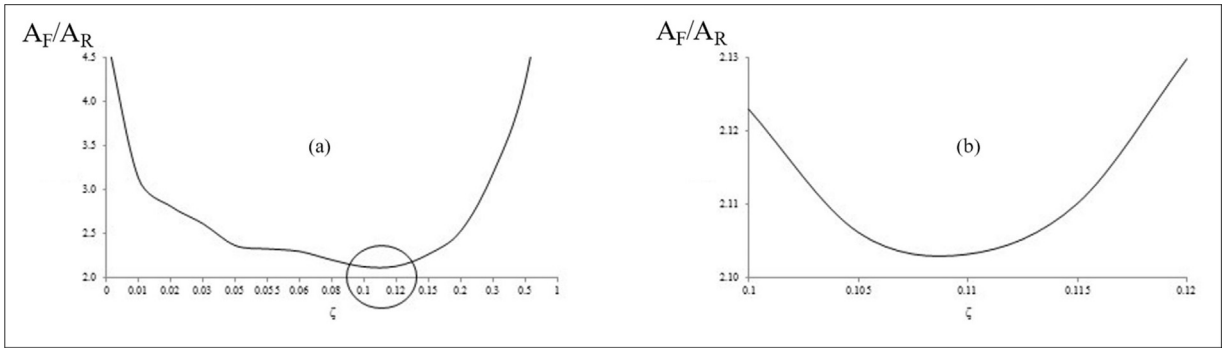


Fig. 2. (a) Curve constructed from the relation of the spectral ordinates as the damping ratio varies from 0 to 1. (b) Curve shape in the approximated minimum interval from 0.1 to 0.12 for increases of 0.005.
Minimum at $\zeta = 0.110$.

In practice, for the same value of ζ, the spectrograms X(T) and F(T) of the two vibration functions x(t) and f(t) are defined by extracting, in correspondence of the value of $T=T_o$, the corresponding amplitudes A_R and A_F and the ratio A_F/A_R [11]. Repeating this operation for n discrete values of ζ between 0 (free vibration) and 1 (overdamped vibration) we obtain the $A_F/A_R(\zeta)$ curve (Fig. 2a).

On the curve, the interval between the two discrete values of ζ that contain the minimum is identified; the calculation is continued within the interval for further increments of ζ until the value that, with the desired numerical approximation, minimizes the previous ratio is determined. In the example, the minimum is found in the interval between 0.10 and 0.12 (Fig. 2a): the calculation is repeated with increments of 0.005, thus the ratios are recalculated for ζ of 0.105, 0.110 and 0.115. Fig. 2b shows the curve within that interval, identifying the definitive minimum at $\zeta = 0.110$: this represents the damping ratio ζ, with a numerical approximation equal to 0.005.

This method is more complex than the one proposed in section 1.2 because it consists of repeatedly calculating the response and external force spectra as ζ varies, in extracting for $T=T_o$ the values of the spectral ordinates A_R and A_F of each pair of spectra, and in plotting the curve $A_F/A_R(\zeta)$ of the corresponding ratios. However, as reported, it has the advantage of a solution independent of the sampling rates of the two functions x(t) and f(t) and of estimating ζ with an approximation that does not depend on the frequency resolution.

In the case studies to be discussed, the buildings or the ties were considered with a single SDOF identifying the mode of vibration around the resonance frequency. It should be noted, however, that this assumption is dictated by the spectral content of the GPS/RTS signals and by the low vibration amplitudes observed since the higher modes and nonlinear effects would not be resolvable.

Moreover, the vibrations were considered with a single SISO (Single Input - Single Output) response (Meirovitch, 1986), for which the structural dynamic model of the building or of the structural element will have the parameters limited to the first mode (Inman, 1996), i.e. to the vibration frequency f_o corresponding to the elastic period of vibration T_o and a single damping ratio ζ.

2. From geodetic and topographical measurements to vibration functions

The steps to pass from the measurements of the geodetic and topographic sensors to the corresponding response functions will now be summarized with reference to the two case studies.

2.1. Geodetic measurements by GPS receivers

The block diagram in Fig. 3 summarizes the steps leading from GPS measurements to calculation of the response vibration functions of the building hosting a permanent GPS receiver.

GPS receivers are situated inside buildings while their antennas are rigidly fixed to the top so that they can receive signals from the GPS constellation without obstructions and continuously throughout the day (Fig. 3a). Therefore, the building's vibration function in response to an excitation (for example an earthquake) is calculated from the instantaneous three-dimensional positions of the antenna's phase center for each sampling rate δt of the receiver, which can vary from a minimum of 1 to a maximum of 20 measurements per second (1 to 20 Hz) (Moschas and Stiros, 2015; Yi et al., 2013). These positions are obtained by processing the raw data in code and phase (Measurement type Dual frequency Code and Phase) and consist of the instantaneous coordinates n,e,u_p in time of the antenna's phase center in the datum of the ephemerides (Fig. 3b). Since this triad has the axes of the plane in directions (tangent to the North meridian and the East parallel) that do not coincide with the directions of the external walls of the building, it is necessary to proceed with a realignment by rigidly rotating them in the direction of its longitudinal and transverse walls (Fig. 3c). The latter constitute the vibration functions at position x(t) of the longitudinal and transverse walls of the building (Fig. 3d) in response to an external excitation: the literature (Psimoulis et al., 2008) considers them affected by an error $3\sigma \leq 0.5$ cm/s. Finally, it is possible to pass from the position response to the velocity response $\dot{x}(t)$ or acceleration response $\ddot{x}(t)$ by deriving once or twice the x(t) with respect to time (Fig. 3e).

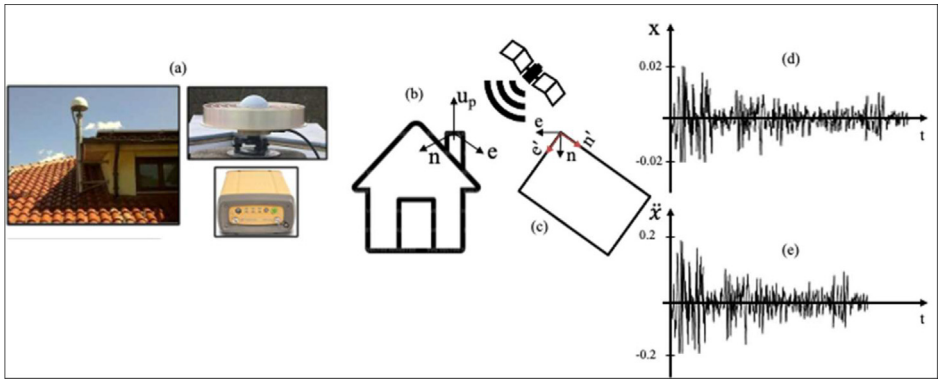


Fig. 3. Block diagram: from GPS measurements to the building's response vibration functions.

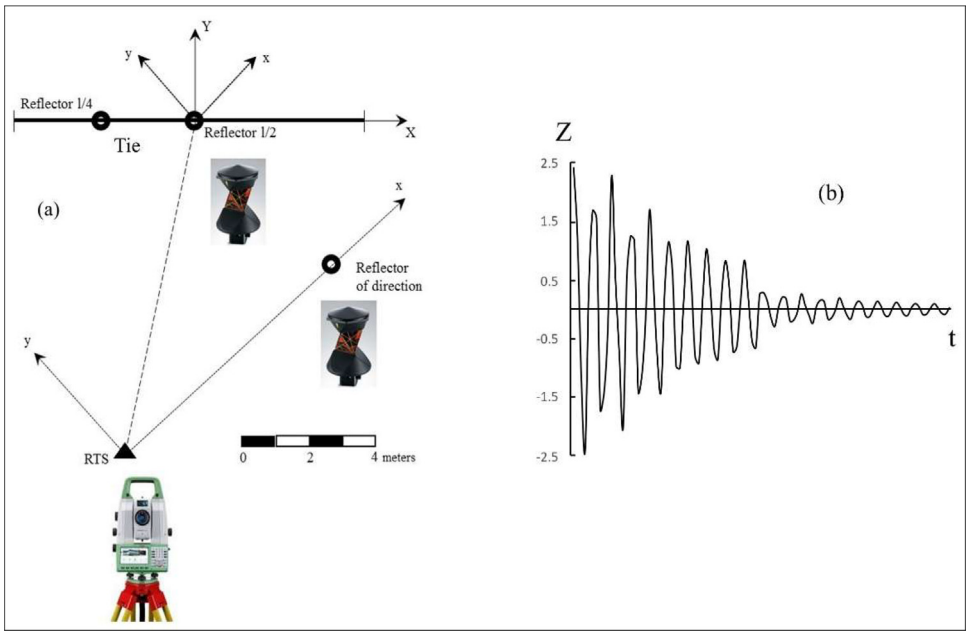


Fig. 4. Measurement schematic: from RTS measurements to the response vibration function of the tie.

2.2. Topographic measurements by a RTS

The RTS is a total station equipped with ultrasonic motors that autonomously collimates (Automatic Target Recognition - ATR) the center of a moving reflector with tracking speeds up to 15°/s and rotation speeds up to 180°/s (Wasmeier, 2003; Leica Geosystems, 2003). Thanks to laser pulse systems with increasingly smaller dot size, the accuracies of measurement of the horizontal Hz and vertical V angles (σ_{Hz} and σ_V) are ca. ±0.5″ (Kirschner and Stempfhuber, 2008) and that of distance (σ_d) is less than ±1 mm + 1 ppm, even in the reflectorless version. The station is provided with an integrated autofocus telescope with wide-angle CMOS cameras (Ehrhart and Lienhart, 2016, 2017), biaxial compensators and temperature and pressure sensors. The recently available RTS have 360° reflectors and triple the sampling rate, up to ca. 10 Hz (Lackner and Lienhart, 2016), so that autocollimations with subcentimetric amplitude variations are possible even in the presence of high vibration frequencies (Di Gregorio et al., 2024; Frukacz et al., 2017).

Fig. 4 shows a measurement schematic of the tie of a vault arch (Fig. 4a) and the representation of a vibration function in the vertical direction Z(t) (Fig. 4b). The measurements are carried out for polar coordinates in space by first collimating a reflector placed in the orientation direction and then, at each time point, collimating (with autocollimation) a second one fixed in the main modal positions of the structure (Fig. 4a) and set in vibration by an impulsive load.

The vibration function Z(t) is obtained by transforming the instantaneous polar coordinates θ,ϕ,d^i into orthogonal Cartesian coordinates (X,Y,Z).

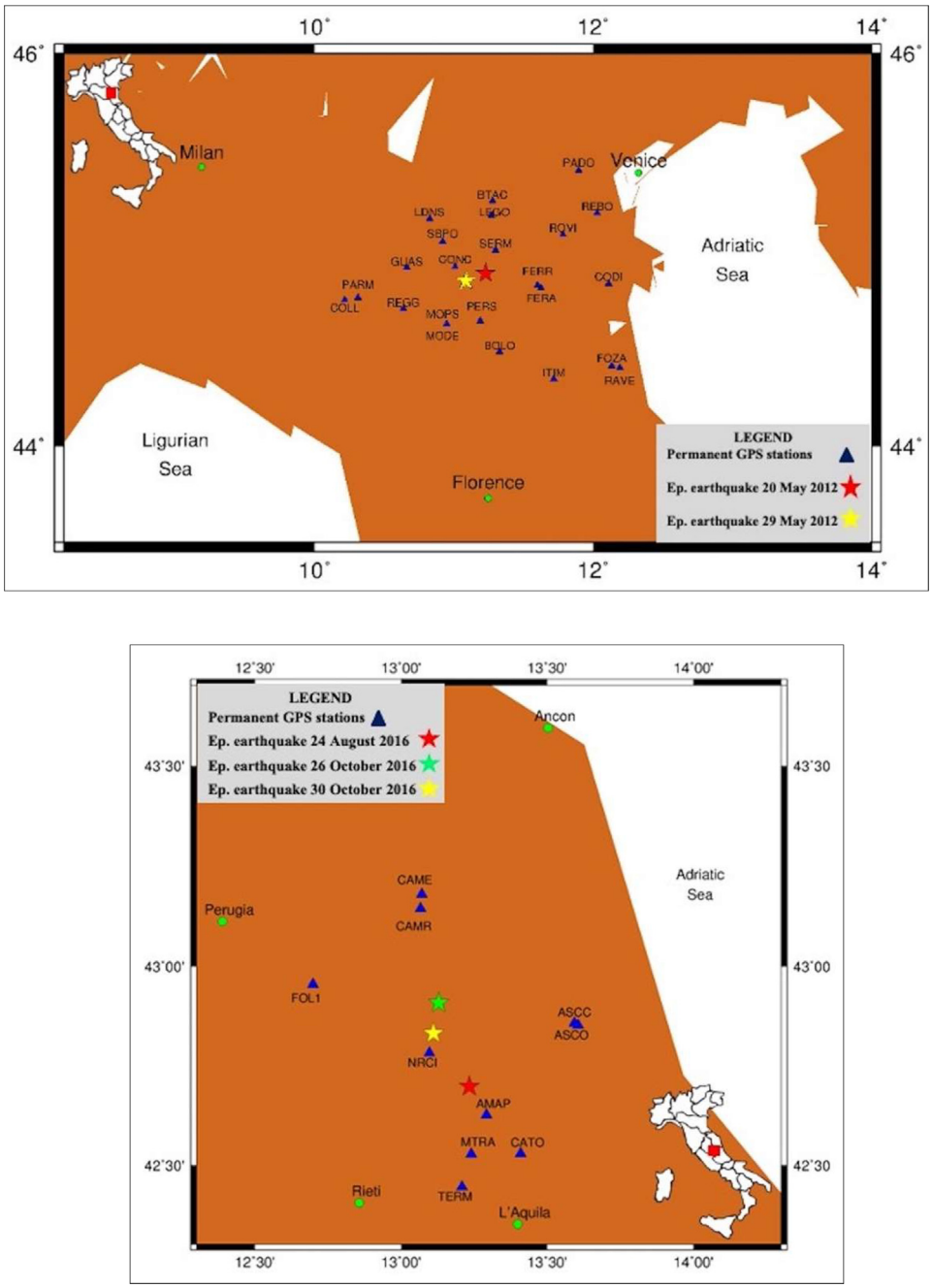


Fig. 5. (above). Permanent GPS stations for the Emilia earthquake 2012.
(below). Permanent GPS stations for the central Italy earthquake 2016.

3. First case study

During the earthquakes in Emilia-northern Italy (Scognamiglio et al., 2012) and central Italy (INGV, 2016), 33 permanent GPS stations (Fig. 5) (Gurtner, 1995) belonging to public and private bodies were active in the area of the epicenters, as were 33 seismic stations of the National Accelerometric Network (RAN) adjacent to them (Table 1).

The permanent stations had an equal number of geodetic GPS/GNSS receivers of multiple constellations (NAVSTAR, GLONASS, GALILEO, etc.) with “choke ring” antennas. The code and phase measurements were coeval with the earthquakes and, in some models, were sampled at up to 10 Hz. The vibration functions of each building in response to the five earthquakes, coincident with the vibrations of their external parts, were calculated in stand-alone ambiguity resolution with the PPP algorithm (Bertiger et al.,

Table 1
Geographic areas, number of permanent GPS stations/buildings, number of RAN stations. Dates of the most intense earthquakes coinciding with the recorded measurements used for the calculation of ζ.

Geographic areas	Permanent GPS stations	RAN seismic stations	Earthquakes
Emilia-northern Italy	23	20	20 May 2012 02:03:53 UTC Mw 5.9 29 May 2012 07:00:03 UTC M_w 5.8
Central Italy	10	13	24 August 2016 01:36:32 UTC M_w 6.0 26 October 2016 19:18:06 UTC M_w 5.9 30 October 2016 06:40:17 UTC M_w 6.5
Total	33	33	5

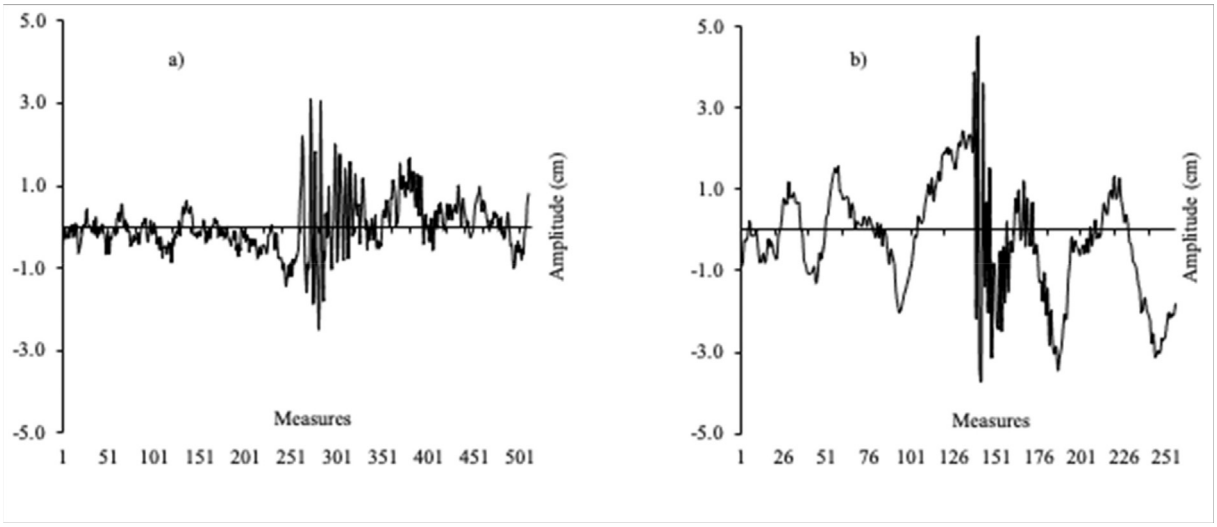


Fig. 6. Example of vibration functions in displacement. a) Emilia-northern Italy earthquake. b) central Italy earthquake.

2010; Psimoulis et al., 2015; Xu et al., 2013; Zumberge et al., 1997) with the calculation code GIPSY OASIS II developed by the Jet Propulsion Laboratory (JPL) (Webb and Zumberge, 1996) in the kinematic positioning (function of time) processing mode: JPL's precise orbit and clock products in the ITRF08 reference system; cut off 5°; average PDOP less than 2; IGS standards satellite antenna phase center offset; antenna calibration file; tropospheric gradients model (Bar-Sever et al., 1998); second order ionospheric delay (Kedar et al., 2003).

Furthermore, since the analysis is focused on estimation of the decrement and of the damping ratio ζ on high-frequency dynamic variations and on limited time windows, corrections for solid Earth tides and ocean tidal loading have not been considered, since tidal effects are characterized by very low-frequency components and, under these conditions, are negligible compared to the content of the analyzed signal.

The processed measurement sample was chosen in multiples of powers of 2 and varied from a minimum of 128 to a maximum of 512.

The shape of the vibration functions showed an almost identical trend, with very small values (even subcentimetric) between the beginning and end of the vibration interspersed with peak concentrations (maximum vibration amplitude in absolute peak value) of higher vibrations, which were repeated for fewer seconds than the former, corresponding to the greatest intensity of the earthquakes (Fig. 6).

In particular, for the Emilia-northern Italy earthquake these peaks had a mean value of 2.5 cm with MSE ±1.1, while the value for the stronger central Italy earthquake was 3.3 cm with MSE ±1.2.

Therefore, for buildings (and not necessarily those farthest from the epicenters) that had low vibration peaks or had high peaks but for short times, it was difficult to reconstruct the damping epoch by epoch because the difference in amplitude between two successive cycles was obscured by the basic GPS measurement error ($\leq$ 0.5 cm/s). It follows that for three buildings of the Emilia Romagna earthquake the logarithmic decrement solution was not applicable, while the measurement accuracy for the spectral response method was irrelevant since the calculation was performed around the maximum spectral ordinate (amplitude) values.

Almost all measurements did not suffer significant cycle slips.

The 33 RAN stations were equipped with triaxial accelerometers from which the accelerometric measurements in the North-South and East-West directions were extracted, with sampling rates at 200 Hz, representing, in acceleration, the external force induced by the earthquake on the buildings.

Table 2a
Elastic period of vibration and damping ratio ζ with MSE for each permanent GPS station. Geographic area of Emilia-northern Italy. Logarithmic decrement method.

Buildings - permanent GPS stations	To (s)	ζ	MSE	ζ %
Bologna (BOLO)	0.57	0.059	0.001	5.9
Concordia (CONC)	0.26	0.052	0.001	5.2
Ferrara (FERA)	0.34	0.084	0.003	8.4
Ferrara (FERR)	0.37	0.076	0.005	7.6
Guastalla (GUAS)	0.24	0.020	0.0001	2.0
Imola (ITIM)	0.51	0.085	0.001	8.5
Legnago (LEGO)	0.35	0.068	0.001	6.8
Mantova (LDNS)	0.32	0.097	0.015	9.7
Modena (MODE)	0.31	0.046	0.004	4.6
Modena (MOPS)	0.33	0.036	0.002	3.6
Padova (PADO)	0.39	0.041	0.002	4.1
Parma (PARM)	0.29	0.063	0.003	6.3
Ravenna (RAVE)	0.28	0.017	0.0003	1.7
Rebosola (REBO)	0.45	0.053	0.0011	5.3
Reggio Emilia (REGG)	0.28	0.013	0.0007	1.3
Rovigo (ROVI)	0.38	0.033	0.0015	3.3
San Benedetto Po (SBPO)	0.33	0.022	0.0014	2.2
San Giovanni in Persiceto (PERS)	0.37	0.066	0.0015	6.6
Sermide (SERM)	0.31	0.045	0.0015	4.5
Verona (BTAC)	0.35	0.073	0.0041	7.3

Table 2b
Elastic period of vibration and damping ratio ζ with MSE for each permanent GPS station. Geographic area of central Italy. Logarithmic decrement method.

Buildings - permanent GPS stations	To (s)	ζ	MSE	ζ %
Amatrice (AMAP)	0.18	0.049	0.0008	4.9
Ascoli Piceno (ASCC)	0.41	0.080	0.0041	8.0
Ascoli Piceno (ASCO)	0.20	0.071	0.0003	7.1
Cagnano Amiterno (TERM)	0.16	0.067	0.0018	6.7
Camerino (CAME)	0.21	0.084	0.0051	8.4
Camerino (CAMR)	0.21	0.075	0.0081	7.5
Campotosto (CATO)	0.15	0.034	0.0004	3.4
Foligno (FOL1)	0.37	0.055	0.002	5.5
Montereale (MTRA)	0.33	0.078	0.0185	7.8
Norcia (NRCI)	0.17	0.036	0.0006	3.6

The acceleration values were recorded in nanometers/sec^2 equivalent to 10^{-7} cm/s^2.
The accelerometric measurements, despite a high sampling rate, also showed no cycle slips.

3.1. Damping ratio calculation

The logarithmic decrement method and the spectral response method were used to calculate the damping ratio ζ. The frequency response method was excluded due to the large difference between the sampling rates of the GPS and accelerometric measurements of the RAN stations.

3.1.1. Logarithmic decrement method

Preliminarily, third- or sixth-order Butterworth band-pass filters with variable range from 0.1 to 50 Hz were applied to each of the response vibration functions at position e'(t),n'(t) calculated along the longitudinal and transverse walls of the buildings (Boore and Akkar, 2003; Lynn and Fuerst, 1998; Stearns and David, 1996). Subsequently, for the filtered functions the number of entire cycles and the corresponding extreme values were identified. For calculation of the logarithmic decrement, they were included in [2] and, from this, the value of ζ was estimated with [3].

The calculation was repeated for each wall and for each earthquake.

Table 2 reports, for the buildings of Emilia-northern Italy (Table 2a) and central Italy (Table 2b), the mean ζ values (with their MSE) calculated between those estimated along the two walls for each of the earthquakes, together with the building's elastic period of vibration.

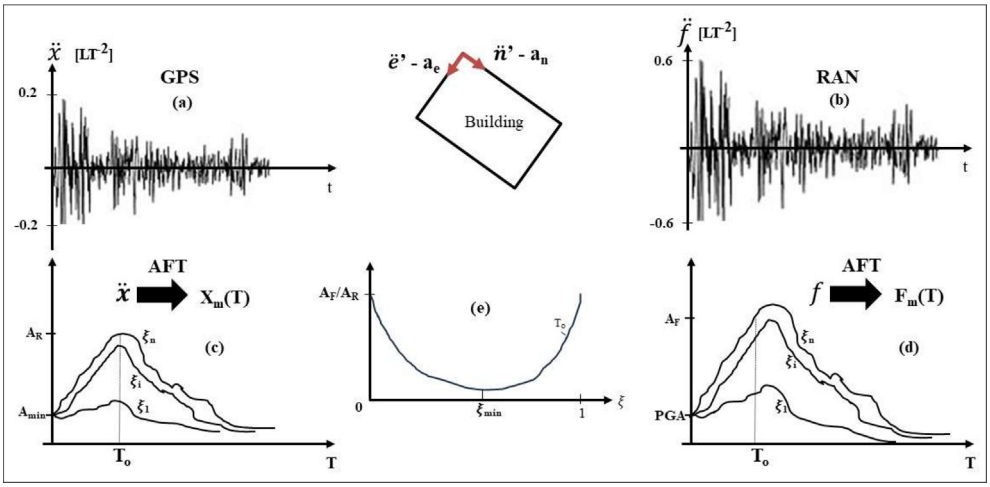


Fig. 7. Spectral response method. Calculation schematic.

3.1.2. *Spectral response method*

Fig. 7 shows the calculation schematic.

The response vibration functions at position e'(t),n'(t) of the longitudinal and transverse walls of the building hosting the permanent GPS station (Fig. 3d) were derived twice with respect to time, obtaining the corresponding vibration functions in acceleration $\ddot{e}(t)$,$\ddot{n}(t)$ (Figs. 3e; 7a).

The vibration functions of the external force, already in acceleration (a_n,a_e), were also rigidly rotated in the same directions. The same filters mentioned in section 3.1.1 were applied to both the former and the latter, transformed into the same measurement units (cm/s^2).

From the two functions, indicated generically as $\ddot{x}(t)$ and $\ddot{f}(t)$, anti-Fourier transforms (AFT) were performed, and the spectrograms X(T) of the response and F(T) of the external force (since there are two vibration functions for both the building and the ground, the spectrograms X(T) and F(T) represent their mean value) were calculated for ζ equal to: 0, 0.01, 0.02, 0.03, 0.05, 0.055, 0.6, 0.8, 0.10, 0.15, 0.20, 0.25, 0.3, 0.5 and 1 (Fig. 7c). From them, for $T=T_o$ of the building, the corresponding spectral ordinates A_R and A_F, the A_F/A_R ratios and the $A_F/A_R(\zeta)$ curves were extracted, obtaining the value of ζ in correspondence of the minimum of the $A_F/A_R(\zeta)$ curve (Fig. 7d).

Since GPS recordings from several earthquakes and measurements from more than one RAN station close to a permanent GPS station were available, the calculation of ζ was repeated several times.

Given the complexity of the calculations and their repetition, the solution was coded in the Matlab environment.

Table 3 reports the mean values of ζ (with their MSE) calculated from those estimated for the five earthquakes and along the two external walls for all the buildings of Emilia-northern Italy (Table 3a) and central Italy (Table 3b).

3.2. *Comparisons*

The first comparison was performed on the damping ratio ζ values reported in Tables 2 and 3: as could be expected, they are practically identical, with differences only at the third decimal place and almost always lower than the estimated MSE; in particular, the mean value $\Delta\zeta_m$ of the differences (in absolute value) in the ζ values of each station reported in Tables 2a–3a and 2b-3b is 0.003 ±0.001 for Emilia-northern Italy and 0.001 ±0.0001 (0.1±0.01%) for central Italy.

It emerged that method 1.1 is less onerous from the point of view of calculation: once the number of entire cycles and the extreme ordinates, i.e. the logarithmic decrement, have been identified for the vibration function, the solution is simple and does not require particular codes. In contrast, method 1.4 is computationally much more laborious: the calculation requires knowledge of the vibration function of the external force and the presence of a complex calculation code is necessary. Nonetheless, its adoption is motivated by the greater robustness in low signal/noise ratio conditions and, when possible, by a more stable identification of the dominant first mode.

Finally, the logarithmic decrement method was not applicable to all the buildings.

The comparisons between the two methods in terms of estimations, calculation costs, calculation times, requirement of a calculation code and application to the case study are summarized in Table 4.

3.3. *Verification of the numerical reliability of the damping ratio ζ values*

No simultaneous or previous measurements with other recording sensors were available. Thus, to verify the numerical reliability of the ζ values obtained with the GPS measurements, an indirect comparison was conducted so as to check the consistency and

Table 3a
Damping ratio ζ with MSE for each permanent GPS station. Geographic area of Emilia-northern Italy. Spectral response method.

Buildings - permanent GPS stations	ζ	MSE	ζ %
Bologna (BOLO)	0.060	0.001	6.0
Codigoro (CODI)	0.055	0.011	5.5
Collecchio (COLL)	0.092	0.048	9.2
Concordia (CONC)	0.051	0.002	5.1
Ferrara (FERA)	0.080	0.006	8.0
Ferrara (FERR)	0.080	0.001	8.0
Guastalla (GUAS)	0.023	0.003	2.3
Imola (ITIM)	0.085	0.002	8.5
Legnago (LEGO)	0.064	0.004	6.4
Mantova (LDNS)	0.100	0.004	10.0
Modena (MODE)	0.048	0.006	4.8
Modena (MOPS)	0.033	0.003	3.3
Padova (PADO)	0.043	0.004	4.3
Parma (PARM)	0.060	0.013	6.0
Ravenna (FOZA)	0.044	0.003	4.4
Ravenna (RAVE)	0.018	0.003	1.8
Rebosola (REBO)	0.051	0.002	5.1
Reggio Emilia (REGG)	0.012	0.001	1.2
Rovigo (ROVI)	0.033	0.002	3.3
San Benedetto Po (SBPO)	0.021	0.003	2.1
San Giovanni in Persiceto (PERS)	0.060	0.006	6.0
Sermide (SERM)	0.040	0.007	4.0
Verona (BTAC)	0.070	0.004	7.0

Table 3b
Damping ratio ζ with MSE for each permanent GPS station. Geographic area of central Italy. Spectral response method.

Buildings - permanent GPS stations	ζ	MSE	ζ %
Amatrice (AMAP)	0.048	0.008	4.8
Ascoli Piceno (ASCC)	0.080	0.0041	8.0
Ascoli Piceno (ASCO)	0.070	0.004	7.0
Cagnano Amiterno (TERM)	0.062	0.002	6.2
Camerino (CAME)	0.084	0.001	8.4
Camerino (CAMR)	0.075	0.002	7.5
Campotosto (CATO)	0.036	0.010	3.6
Foligno (FOL1)	0.053	0.010	5.3
Montereale (MTRA)	0.075	0.011	7.5
Norcia (NRCI)	0.036	0.005	3.6

Table 4
Comparisons of the two methods.

Method	Estimations	Calculation	Calculation times	Vibration function of the external force	Calculation code	Application
Logarithmic decrement	Identical	Limited	Short	Not necessary	Not relevant	Partial
Spectral response	Identical	Laborious	Long	Necessary	Necessary	Total

plausibility in terms of order of magnitude. It was carried out with values from the literature and thus is limited to equivalent construction material and height of the buildings.

The buildings hosting the permanent GPS stations in Emilia-northern Italy were predominantly made with reinforced concrete frames, while those in central Italy were prevalently in masonry. Images of some buildings are included in Fig. 8 to show the construction material and height.

Of the buildings studied, 12 were made of masonry and 21 of reinforced concrete. In Table 5 the mean ζ values extracted from Tables 2 and 3 are reported as a function of the construction material.

These values are consistent with those of Engineering Sciences Data Unit ESDU (1991) (reported by Elnashai and Di Sarno, 2008 in their Table 2.9) which, for buildings in general, reports a value of 5%. In Bachmann et al (1995) (also cited by the preceding authors in their Table 2.6) the indicated values are between 5 and 8%. Also in Lin et al (2005) and Rao (2011), for reinforced concrete only, the values are from 4% to 8%, in line with those reported in Table 5.



Fig. 8. Images of some buildings hosting permanent GPS stations.

Table 5
Mean value of ζ according to the construction material: masonry and reinforced concrete.

Construction material	No. buildings	ζ	ζ %
Masonry	12	0.064	6.4
Reinforced concrete	21	0.063	6.3

Table 6
Mean value of the damping ratio ζ according to the height.

H (m)	No. buildings	ζ	ζ %
4	5	0.065	6.5
6	10	0.057	5.6
9	11	0.057	5.7
12	5	0.056	5.7
15	2	0.056	5.7

For the geometry, heights were taken into consideration, ranging from a minimum of 4 m (single-story buildings) to a maximum of 15 m (buildings with 5 stories above ground). Table 6 reports the corresponding mean ζ value extracted from Tables 2 and 3.

The ζ values reported in Table 6 are consistent with what was reported by Satake et al (2003), who for 25 reinforced concrete buildings estimated a damping ratio ζ of the first vibration mode for the first 15 m that decreased with height, with values from 8 to 6%.

4. Second case study

During assessment of the tension of four steel ties set in the masonry arches of a church (Fig. 9), the vibration functions Z(t) of the ties in the vertical direction were measured with a robotic total station.

Since the work specifically focuses on the use of topographic sensors for the dynamic monitoring of structures, the second case study was introduced as a complementary analysis carried out under controlled conditions. Therefore, the vibration functions Z(t) in the vertical direction of the ties were measured to support and interpret the results obtained in the first case study, based on real seismic responses.

The top-range RTS had the following characteristics:

- Sampling rate up to 10 Hz, achieved with a proprietary firmware upgrade:
- Angle measurement absolute accuracy: σ_{Hz} and $\sigma_V = \pm 0.5''$ (± 0.15 mgon);
- Distance measurement accuracy with prism: $\sigma_d = \pm 0.6$ mm + 1 ppm;
- Laser dot size at 50 m: 8 mm × 20 mm;
- Measurement technology: system analyzer, coaxial, visible red laser;
- Image: sensor CMOS 5 megapixel; field of view (overview/telescope) 19.4°/1.5°; frame rate up to 20 frames per second;
- Motorization direct drives based on piezo technology: rotation speed/time to change face; maximum 180°/second;
- Automatic aiming – ATR: accuracy/measurement time ATR angle accuracy σ_{Hz} and $\sigma_V = \pm 0.5''$ (± 0.15 mgon);
- 360° degree reflectors;
- Power search: range/search time 360° prism 300 m.

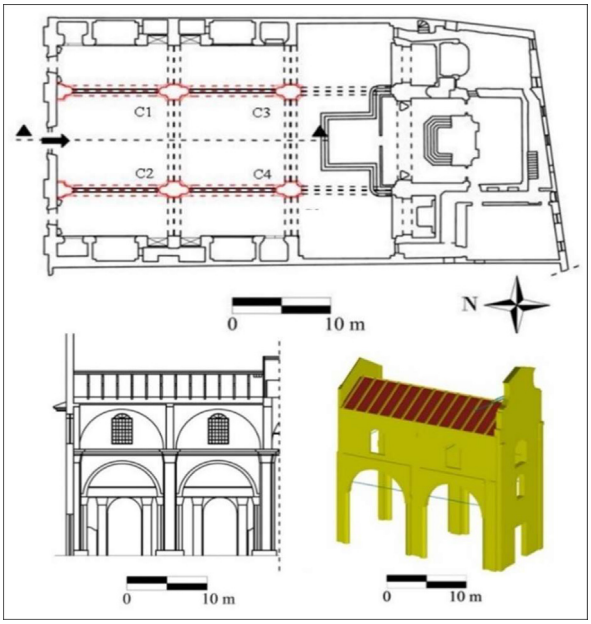


Fig. 9. Plan with identification of the ties. Section of the arches and 3D view.

The measurements were performed with the following modalities, at a distance of ca. 20 m, with the reflector positioned at half the tie's length (Fig. 4):

- autocollimation of the reflector of direction;
- autocollimation and recording of the polar coordinates θ,ϕ,d^i of the reflector's center with the tie stationary;
- application of an impulsive load obtained by vertical pulling of a steel cable anchored to the top of the tie close to the reflector;
- autocollimation and recording of the polar coordinates θ,ϕ,d^i of the center of the reflector with the tie in vibration, with a sampling rate of 10 Hz.

The pulls were repeated on average five times; after the pull the vibration lasted ca. 5 s and then the reflector was allowed to return to the equilibrium position for 5 s. Hence the duration of a measurement session was ca. 50 s, equivalent to ca. 500 measurements. The complete sessions varied from a minimum of 4 and a maximum of 6.

At the end of the measurements, the instantaneous polar coordinates θ,ϕ,d^i were transformed into orthogonal cartesian coordinates (X,Y,Z).

Prior to calculation of the vibration functions, the capability of the RTS to continuously record and the accuracy of the differences (in absolute value) of the Z coordinate between two successive sampling intervals were evaluated.

With regard to the continuous recording in autocollimation, the number of recorded measurements and their difference (cycle slip) from the expected measurements were calculated for each tie and for each measurement session. Fig. 10 reports the cycle slips (as percentage) for each tie and for each measurement session.

The cycle slips vary from a minimum of 3% to a maximum of 15%, with a mean of ca. 8%. The maximum cycle slips occurred when the Z(t) vibrations reversed their sign and the vibration amplitudes decreased.

To evaluate the applicability of the proposed methods to the Z(t) coordinate, the peak values (maximum vibration amplitude in absolute value) and peak-to-peak (sum of the two maximum positive and negative vibration amplitudes, the latter in absolute value) were considered. During the pulls, there was a maximum peak of 3.3 mm (average 3.1 ± 0.2 mm) and a maximum peak-to-peak of 6.3 mm (average 5.8 ±0.4 mm) for which the value of the mean decrease between two successive epochs was ~0.6 mm. Considering that the RTS measures the Z coordinate with an accuracy of $3\sigma_Z = \pm$ 0.2 mm at a distance of ca. 20 m and in accordance with the accuracies declared by the manufacturer (σ_V ±0.5″ and σ_d ±0.6 mm + 1 ppm), this decrease is clearly resolvable and distinguishable from the measurement noise. Therefore, despite the low frequency vibrations of the four ties, it was possible to obtain from a RTS with 10 Hz sampling rate vibration functions with decreases between two successive epochs that are higher than the instrumental accuracy, allowing a reliable estimation of the damping ratio ζ.

Consequently, with the vibration functions of the Z coordinate of the reflector placed at the tie's midpoint, the damping ratio ζ was calculated with the logarithmic decrement and frequency domain decomposition methods.

Fig. 11 shows an example of the vibration function Z(t) of tie C_1: the time t (in seconds) refers to the duration of session I while the vertical grid highlights the moments between one pull and the next one. The peak is reached at the moment of the pull, after which the amplitude decreases in a few seconds until the equilibrium condition is reached.

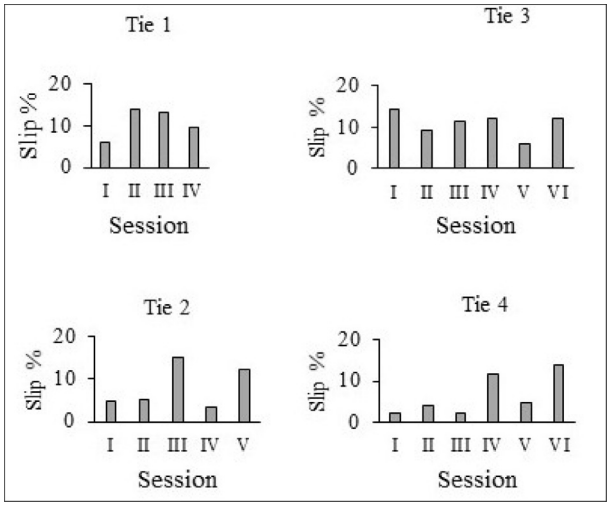


Fig. 10. Cycle slips (as percentage) per tie and measurement session.

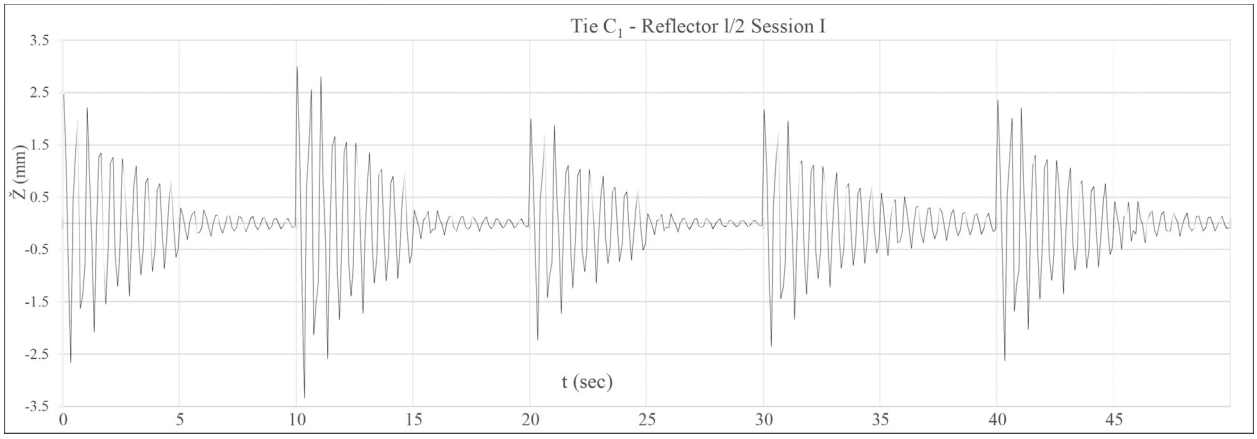


Fig. 11. Examples of representation of the experimental hourly diagrams of the vertical vibrations of tie C_1.
On the abscissa, the time t (*sec*) refers to the entire duration of a measurement session.
The vertical vibration $\hat{Z}(t)$ (mm) is on the ordinate.
The vertical grid shows the moments between one pull and the next one.

4.1. Damping ratio calculation

To calculate the damping ratio ζ, the logarithmic decrement and frequency domain decomposition methods were chosen, since both method 1.2 and method 1.4 were inapplicable due to the lack of the vibration function of the external force. The vibration functions were preliminarily filtered for values lower than the accuracy (minimum threshold of ±0.6 mm) and interpolated in correspondence of cycle slips: in this way, recording shifts were absent or in negligible number in the Z(t). The entire cycles and the extreme values were identified between the beginning and end of a single pull, i.e. every 5 s. The estimation of ζ at the midpoint of the ties was repeated in all measurement sessions.

4.1.1. Logarithmic decrement method

Table 7 shows the values of ζ with MSE obtained with the logarithmic decrement method.

4.1.2. Frequency domain decomposition method

A further filter, an 8th-order Chebyshev filter with cut-off frequency of 0.1 Hz, was applied to the vibration functions, and the PSD was extracted with a frequency amplitude of 0.02 Hz, while the NExT algorithm was used for the solution of ζ (James, 1995): also in this case the calculation was coded in the Matlab environment. Table 8 reports, for each tie, the values of the frequencies f and of ζ, with their MSE.

Table 7
Damping ratio ζ with MSE for each of the four ties. Logarithmic decrement method.

Tie	ζ	ζ%
C_1	0.010 ± 0.002	1
C_2	0.011 ± 0.001	1.1
C_3	0.009 ± 0.004	0.9
C_4	0.008 ± 0.003	0.8

Table 8
Frequencies and damping ratio ζ with MSE for each of the four ties. Frequency domain decomposition method.

Tie	f (Hz)	ζ	ζ%
C_1	2.01	0.009 ± 0.0018	0.9
C_2	2.10	0.009 ± 0.0011	0.9
C_3	3.69	0.009 ± 0.0008	0.9
C_4	2.01	0.009 ± 0.0020	0.9

Table 9
Comparisons of the logarithmic decrement and frequency domain decomposition methods.

Method	Estimations	Calculation	Calculation times	Vibration function of the external force	Calculation code	Application
Logarithmic decrement	Identical	Limited	Short	Not necessary	Not relevant	Total
Frequency domain decomposition	Identical	Laborious	Medium	Not necessary	Necessary	Total

4.2. Comparisons

The first comparison was carried out for the ζ values reported in Tables 7 and 8: the values obtained with the two methods differ by a mean value of $\Delta\zeta_m = 0.00005 \pm 0.00001$ (0.005 ± 0.001%).

Method 1.3 has lower calculation costs if standard calculation libraries are available, so the presence of a complex code can be limited. Since it is linked to the preliminary calculation of the mode frequencies, it requires that the measurements be sampled with an interval at least double the corresponding mode frequency. The vibration functions of the ties showed regular shapes (Fig. 4b and Fig. 11) also for subcentimetric amplitudes; hence, since it was easy to identify the decreases and the peaks in frequency, application of the two solutions to the case study was total.

The comparisons between the two methods in terms of estimations, calculation costs, calculation times, requirement of a calculation code and application to the case study are summarized in Table 9.

4.3. Verification of the numerical reliability of the damping ratio ζ values

The ζ values reported in Tables 7 and 8 were compared with those extracted from the vibration functions measured on the ties with monoaxial piezoelectric accelerometers; the ties were made to vibrate by striking them with an impulse hammer (Force) weighing a few kilograms. Fig. 12 reports the measurement schematic with graphs of the vibration function of the external force and of the responses.

Multiple recordings and measurement sessions were performed, with the accelerometers positioned at $\frac{1}{2}$ and $\frac{1}{4}$ the tie's length. Prior to application of the methods, the vibration functions were obtained by filtering the recordings with a 4th-order Chebyshev bandpass filter with cut-off frequencies from 0.1 to 25 Hz. Since the vibration functions of the response and the external force of the ties were sampled at the same rate, the bandwidth solution indicated in the frequency response method was used to estimate the damping ratio ζ. Table 10 reports the results.

The mean of the differences between the ζ values reported in Tables 7 and 8 and those reported in Table 10 differ by a mean of $\Delta\zeta_m = 0.0002 \pm 0.0001$ (0.02 ± 0.01%).

Conclusions

In the case of GPS measurements, the presence of low amplitudes that were confused with the measurement noise made identification of the damping ratio ζ more complex; thus the logarithmic decrement method was not applied to all the buildings. The frequency response method is conditional on knowledge of the vibration function of the external force and on the fact that both vi-

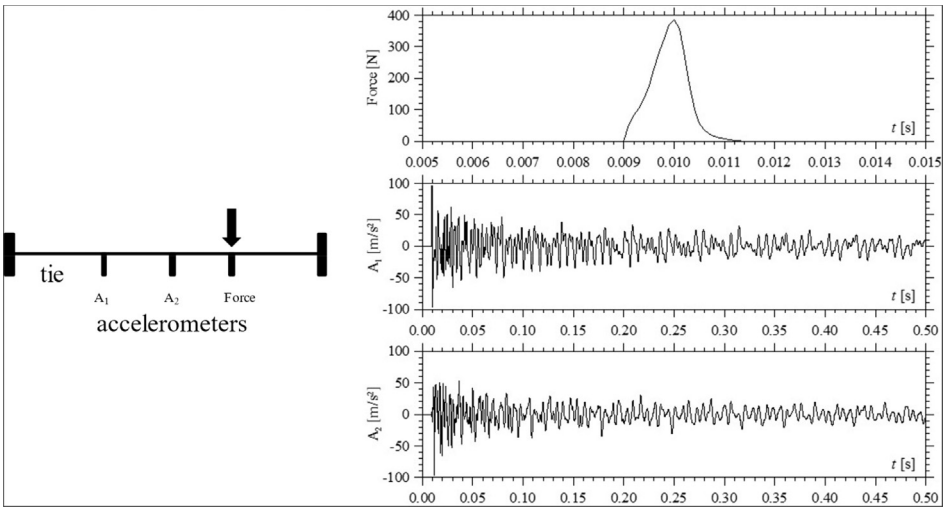


Fig. 12. Schematic of the measurement with graphs of the vibration functions of the external force and the responses.

Table 10
Calculation of ζ with accelerometric measurements and impulse hammer. Frequency response method.

Tie	ζ	ζ%
C_1	0.011	1
C_2	0.014	1
C_3	0.010	1
C_4	0.012	1

bration functions must be sampled in the same way; therefore since GPS measurements were compared with much higher frequency accelerometric measurements it was not possible to apply it. Vice versa, the spectral response method is totally applicable to these measurements both because it is not necessary that the external force and the response have the same sampling rate and, above all, because the value of the damping ratio ζ is extracted in correspondence of the values of the maximum spectral ordinates (amplitudes), so their accuracy becomes irrelevant, also in accordance with the adoption of the SDOF model aimed exclusively at estimation of the damping ratio ζ of the first vibration mode.

The vibration functions of the ties deduced from the RTS measurements presented regular shapes (albeit with cycle slips especially when they inverted the sign and the amplitudes decreased in value). During the pulls, they reached decreases higher than the accuracies declared by the manufacturer; hence it was possible to extract the ζ values both with the logarithmic decrement method and with the frequency domain decomposition method.

Regarding the calculation costs and times for the recorded measurements, the computationally less onerous logarithmic decrement method did not require particular calculation sequences. In contrast, both the frequency domain decomposition and spectral response methods were more laborious, making necessary the use of a dedicated calculation code.

Consequently, the use of more computationally complex methods was not aimed at obtaining numerically different damping values, but rather at ensuring greater robustness in the analysis of real monitoring data, particularly in low signal-to-noise ratio conditions and, when possible, a more stable identification of the dominant first vibration mode.

The values of ζ estimated for each case study and for each method were numerically similar, and their comparison with values reported in the scientific literature confirmed their consistency in terms of order of magnitude.

In the logarithmic decrement and frequency domain decomposition methods, the precision with which ζ was estimated depended on the frequency amplitude, which in turn is linked to the sampling rate. Hence the maximum sampling rates currently possible in both GPS and RTS measurements (ca. 10 Hz) are still a limitation to use in all the adopted methods.

Finally, the exclusion of some methods in the specific case studies is linked to practical constraints (for example the absence of the function of the external force or discrepancies in sampling rates) but not to the approaches used. Thus, although the analyzed methods were not fully applied under all investigated conditions, their comparison should be interpreted within the scope of the present study.

Declaration of competing interest

The author does not have a relevant conflict of interest to declare for this article.

CRediT authorship contribution statement

Marco Gatti: Methodology, Formal analysis, Data curation, Conceptualization.

Acknowledgments

Thanks go to the Civil Protection Department and the National Institute of Geophysics and Volcanology for having provided the data of the RAN network accelerometric stations, and to the Universities and public research bodies as well as the companies Leica and Topcon for the data of the permanent GPS stations.

Data availability statement

The data processed by the author in this paper are available upon request to him.

References

Adhikari, S., 2013. Structural Dynamic Analysis with Generalized Damping Models. John Wiley & Sons.
Andrianne, T., Dimitriadis, G., 2012. Damping identification of lightly damped linear dynamic systems using common-base proper orthogonal decomposition. Mech. Syst. Signal Process. 28, 492–506.
Bachmann, H., Ammann, W.J., Deischl, F., et al., 1995. Vibration Problems in Structures. Practical Guidelines. Birkhauser Verlag, Basel Switzerland.
Bar-Sever, Y.E., Kroger, P.M., Borjesson, J.A., 1998. Estimating horizontal gradients of tropospheric path delay with a single GPS receiver. J. Geophys. Res. 103, 5019–5035.
Beards, C., 1996. Structural Vibration: analysis and Damping. Elsevier.
Béliveau, J.G., 1976. Identification of viscous damping in structures from modal information. J. Appl. Mech. 43 (2), 335–339.
Bert, C.W., 1973. Material damping: an introductory review of mathematic measures and experimental technique. J. Sound Vib. 29 (2), 129–153.
Bertiger, W., Desai, S.D., Haines, B., et al., 2010. Single receiver phase ambiguity resolution with GPS data. J. Geod. 84, 327–337.
Blandon, C.A., Priestley, M.J.N., 2005. Equivalent viscous damping equations for direct displacement-based design. J. Earthq. Eng. 9 (2), 257–278.
Boore, D.M., Akkar, S., 2003. Effects of causal and acausal filters on elastic and inelastic response spectra. Earthq. Eng. Struct. Dyn. 32, 1729–1748.
Breuer, P., Chmielewski, T., Górski, P., Konopka, E., Tarczyński, L., 2015. Monitoring horizontal displacements in a vertical profile of a tall industrial chimney using global positioning system technology for detecting dynamic characteristics. Struct. Control Health Monit. 22 (7), 1002–1023.
Brincker, R., Zhang, L., Andersen, P., 2000. Modal identification from ambient responses using frequency domain decomposition. In: IMAC 18 Proceedings of the Internatonal Modal Analysis Conference (IMAC), San Antonio, Texas, USA, pp. 625–630 2000.
Brincker, R., Zhang, L., Andersen, P., 2001. Modal identification of output-only systems using frequency domain decomposition. Smart Mater. Struct. 10 (3), 441.
Brownjohn, J.M.W., Koo, K.Y., Scullion, A., List, D., 2012. Operational deformations in Long Span Bridges Bridge maintenance, safety, management, resilience and sustainability. In: Proceedings of the Sixth International IABMAS Conference. Stresa, Lake Maggiore, Italy.
Bürki, B., Guillaume, S., Sorber, P., and Oesch, H.P., 2011. DAEDALUS: A versatile digital clip-on measuring syst. For total stations. Swiss national report on the geodetic activities in the years 2007 to 2011: presented to the XXV General Assembly of the International Union of Geodesy and Geophysics in Melbourne, Australia, 153–156.
Charalampous, E., Psimoulis, P., Guillaume, S., et al., 2015. Measuring sub-mm structural displacements using QDaedalus: a digital clip-on measuring system developed for total stations. Appl. Geom. 7, 91–101.
Chen, S.Y., Ju, M.S., Tsuei, Y.G., 1996. Estimation of mass, stiffness and damping matrices from frequency response functions. J. Vib. Acoust. 118 (1), 78–82.
Chopra, A.K., 1995. Dyn. of Structures: Theory and Applications to Earthquakes Engineering. Prentice-Hall Inc. Upper Saddle River, New York.
Clough, R.W., Penzien, J., 1993. Dynamics of Structures. McGraw Hill, New York.
Cosser, E., Roberts, G.W., Meng, X., Dodson, A.H., 2003. Measuring the dynamic deformation of bridges using a total station. In: Proceedings of the 11th fig Symposium on Deformation Measurements. Santorini, Greece Vol. 25.
Crandall, S.H., 1970. The role of damping in vibration theory. J. Sound Vib. 11 (1), 3 3-IN1.
Dalenbring, M., 1999. Damping function estimation based on measured vibration frequency responses and finite-element displacement modes. Mech. Syst. Signal. Process. 13 (4), 547–569.
Denißen, J., Koskela, A., Mena, H., Tomljanovic, Z., 2014. Damping optimization in vibrational systems based on amplitude. In: The 21th International Symposium on Mathematical Theory of Networks and Systems, pp. 1222–1227.
Di Gregorio, R., Gatti, M., Simas, H., Simoni, R., 2024. Parallel pointing syst. Suitable for robotic total stations: selection, dimensional synthesis, and accuracy analysis. Machines 12 (54), 1–21.
Ding, Y., Law, S.S., 2011. Structure damping identification based on an iterative regularization method. J. Sound Vib. 330 (10), 2281–2298.
Ehrhart, M., Lienhart, W., 2016. Accurate measurements with image-assisted total stations and their prerequisites. J. Surv. Eng., 04016024.
Ehrhart, M., Lienhart, W., 2017. Object tracking with robotic total stations: current technologies and improvements based on image data. J. Appl. Geod. 11 (3), 131–142.
Ehrhart, M., Lienhart, W., Grick, M., 2016. High frequent total station measurements for the monitoring of bridge vibrations. In: Proceedings of the 3rd Joint Internatonal Symposium on Deformation Monitoring. Vienna, Austria 2016.
Elnashai, A.S., Di Sarno, L., 2008. Fundamentals of Earthquakes Engineering. John Wiley & Sons, Chichester UK.
Engineering Sciences Data Unit ESDU, 1991. Parameters Used in Response Calculations (Estimation of Numerical Values). ESDU, London UK.
Ewins, D.J., 1984. Modal Testing: Theory, Practice and Application. 2nd Edition July 2009 400 Pages. John Wiley & Sons, New York.
Fabunmi, J., Chang, P., Vorwald, J., 1988. Damping matrix identification using the spectral basis technique. J. Vib. Acoust. Stress Reliab. Des. 110, 332–337.
Fang, J.Q., Li, Q.S., Jeary, A.P., Liu, D.K., 1999. Damping of tall buildings: its evaluation and probabilistic characteristics. Struct. Des. Tall Spec. Build. 8 (2), 145–153.
Frukacz, M., Presl, R., Wieser, A., Favot, D., 2017. Pushing the sensitivity limits of RTS-based continuous deformation monitoring of an alpine valley. Appl. Geom. 9, 81–92.
Gatti, M., 2018. Peak horizontal vibrations from GPS response spectra in the epicentral areas of the 2016 earthquake in central Italy. Geomat. Nat. Hazards Risk. 9 (1), 403–415.
Gatti, M., 2022. Measurement of vibration frequencies of ties in masonry arches by means of a robotic total station. Earthq. Eng. Eng. Vib. 21 (2), 489–500.
Geosystems, L., 2003. TPS info-Kalibrierung. TPS info-Kalibrierung, 11. Leica TPS Info.
Géradin, M., Rixen, D., 1997. Mechanical Vibrations:- Theory and Application to Structural Dynamics. 3rd Edition May 2012. John Wiley & Sons, New York, p. 500.
Gurtner, W., 1995. Guidelines for a permanent EUREF GPS network. In: Proceedings of the EUREF Symposium, Helsinki, Finland, EUREF Publication No. 4, Editor E. Gubler and H. Hornik.
Hermans, L., Van Der Auweraer, H., Guillaume, P., 1998. A frequency-domain maximum likelihood approach for the extraction of modal parameters from output-only data. In: Proceedings of the International Conference on Noise and Vibration Engineering (ISMA-23), Leuven (Belgium), pp. 367–376 September 16-18, 1998.
INGV. National Institute of Geophysics and Volcanology, 2016. Summary Report on the 30 October 2016 Earthquakes in Central Italy Mw 6.5. Rome, 2016, 1-49.

Inman, D.J., 1996. Engineering Vibration. Prentice Hall, Englewood Cliffs, New Jersey, 1996. 2nd edition.
Jakovčević Stor, N., Slapničar, I., Tomljanović, Z., 2022. Fast computation of optimal damping parameters for linear vibrational systems. Mathematics 10 (5), 790.
James, G.H., 1995. The natural excitation technique (NExT) for modal parameter extraction from operating structures. IJAEM 10 (4), 260.
Jeary, A.P., 1986. Damping in tall buildings - a mechanism and a predictor. Earthq. Eng. Struct. Dyn. 14 (5), 733–750.
Kedar, S., Hajj, G.A., Wilson, B.D., Heflin, M.B., 2003. The effect of the second order GPS ionospheric correction on receiver positions. Geophys. Res. Lett. 30 (16), 1829.
Kirschner, H. and Stempfhuber, W., 2008. The kinematic potential of modern tracking total stations - A state of the art report on the Leica TPS 12001. In: Proceedings of the 1st International Conference Machine Control and Guidance, H. Ingensand, W. Stempfhuber, Eds., Eidgenössische Technische Hochschule (ETH), Zurich, Switzerland, 1-10.
Lackner, S., Lienhart, W., 2016. Impact of prism type and prism orientation on the accuracy of automated total station measurements. In: Proceedings of the Joint International Symposium on Deformation Monitoring. Vienna-Austria.
Li, H.N., Yi, X.D., Yi, T.H., et al., 2004. Real-time monitoring and data analysis of long-span bridge based on GPS and total station technology. In: Proceedings of the Third China-Japan-US Symposium on Structures Health Monitoring and Control. Dalian, China.
Li, X.Y., Law, S.S., 2009. Identification of structural damping in time domain. J. Sound Vib. 328 (1-2), 71–84.
Lin, Y.Y., Miranda, E., Chang, K.C., 2005. Evaluation of damping reduction factors for estimating elastic response of structures with high damping. Earthq. Eng. Struct. Dyn. 34 (11), 1427–1443.
Liu, K., Kujath, M.R., Zheng, W., 2000. Quantification of non-proportionality of damping in discrete vibratory systems. Comput. Struct. 77 (5), 557–570.
Lynn, P.A., Fuerst, W., 1998. Introductory Digital Signal Processing with Computer Applications. Wiley & Sons.
Maia, N.M.M., Silva, J.M.M., Ribeiro, A.M.R., 1998. On a general model for damping. J. Sound Vib. 218 (5), 749–767.
Maximov, Y., Legovich, Y., Maximov, D., 2021. Frequency characteristics of viscoelastic damper models and evaluation of a damper influence on induced oscillations of mechanical system elements. Meccanica 56, 3107–3124.
Meirovitch, L., 1986. Elements of Vibration Analysis. McGraw-Hill, New York.
Meirovitch, L., 1997. Principles and techniques of vibrations. Prentice Hall Int., NJ.
Min, C., Park, H., Park, S., 2012. Direct identification of non-proportional modal damping matrix for lumped mass system using modal parameters. J. Mech. Sci. Technol. 26, 993–1002.
Minas, C., Inman, D.J., 1991. Identification of a nonproportional damping matrix from incomplete modal information. J. Vib. Acoust. 113, 219–224.
Moschas, F., Stiros, S.C., 2013. Three-dimensional dynamic deflections and natural frequencies of a stiff footbridge based on measurements of collocated sensors. Struct. Control Health Monit. 21, 23–42.
Moschas, F., Stiros, S.C., 2014. Rapid decay of a timber footbridge and changes in its modal frequencies derived from multiannual lateral deflection measurements. J. Bridge Eng. 19 (12), 05014005.
Moschas, F., Stiros, S.C., 2015. Dynamic deflections of a stiff footbridge using 100-hz GNSS and accelerometer data. J. Surv. Eng. 141 (4), 04015003.
Muravyov, A., 1998. Forced vibration responses of a viscoelastic structure. J. Sound Vib. 218 (5), 892.
Muscia, R., 1991. A theoretical experimental method based on modal analysis for estimating the damping capacity of vibrating structures. Mech. Syst. Signal Process. 5 (6), 475–499.
Nakić, I., 2013. Optimal damping of the infinite-dimensional vibrational systems: commutative case. Glas. Mat. 48 (2), 373–390.
Paz, M. and Saunders, S.H., 1985. Structural dynamics. Theory and computation. 2nd Edition, Van Nostrand Reinhold.
Phani, A.S., Woodhouse, J., 2007. Viscous damping identification in linear vibration. J. Sound Vib. 303 (3-5), 475–500.
Phani, A.S., Woodhouse, J., 2009. Experimental identification of viscous damping in linear vibration. J. Sound Vib. 319 (3-5), 832–849.
Pradhan, S., Modak, S.V., 2012. A method for damping matrix identification using frequency response data. Mech. Syst. Signal Process. 33, 69–82.
Prandina, M., Mottershead, J.E., Bonisoli, E., 2009. An assessment of damping identification methods. J. Sound Vib. 323 (3-5), 662–676.
Prells, U., Friswell, M.I., 2000. A measure of non-proportional damping. Mech. Syst. Signal Process. 14 (2), 125–137.
Psimoulis, P., Houlie, N., Meindl, M., Rothacher, M., 2015. Consistency of PPP GPS and strong-motion records: case study of Mw 9.0 Tohoku-Oki 2011 earthquake. Smart Struct. Syst. 16 (2), 347–366.
Psimoulis, P., Peppa, I., Bonenberg, L., Ince, S., Meng, X., 2016. Combination of GPS and RTS Measurements for the Monitoring of Semi-Static and Dynamic Motion of Pedestrian Bridge. 3rd Joint Int. Symposium on Deformation Monitoring.
Psimoulis, P., Pytharouli, S., Karambalis, D., Stiros, S.C., 2008. Potential of Global Positioning System (GPS) to measure frequencies of oscillations of engineering structures. J. Sound Vib. 318 (3), 606–623.
Psimoulis, P., Stiros, S.C., 2012. Response of a historical short-span railway bridge to passing trains: 3-D deflections and dominant frequencies derived from Robotic Total Station (RTS) measurements. Eng. Struct. 45, 362–371.
Psimoulis, P., Stiros, S.C., 2013. Measuring deflections of a short-span railway bridge using a robotic total station. J. Bridge Eng. 18, 182–185.
Radovanovic, R.S., Teskey, W.F., 2001. Dynamic monitoring of deforming structures: GPS versus robotic tacheometry systems. In: Proceedings of the 10th FIG International Symposium on Deformation Measurements, pp. 61–70.
Rao, S.S., 2011. Mechanical Vibrations. Fifth Edition. Prentice Hall, Indianapolis, IN.
Satake, N., Suda, K.I., Arakawa, T., Sasaki, A., Tamura, Y., 2003. Damping evaluation using full-scale data of buildings in Japan. J. Struct. Eng. 129 (4), 470–477.
Scognamiglio, L., Margheriti, L., Mele, F.M., et al., 2012. The 2012 Pianura Padana Emiliana seismic sequence: locations, moment tensors and magnitudes. Ann. Geophys. 55 (4), 549–559.
Segalman, D.J., 1987. Calculation of damping matrices for linearly viscoelastic structures. J. Appl. Mech. 54, 585–588.
Sivaprasad, R., Venkatesha, S., Manohar, C.S., 2009. Identification of dynamical systems with fractional derivative damping models using inverse sensitivity analysis. Comput. Mater. Contin. 9 (3), 179.
Stache, N.C., Zimmer, H., 2007. Robust circle fitting in industrial vision for process control of laser welding. In: Proceedings 11th International Student Conference on Electrical Engineering. Prague.
Stearns, S., David, R., 1996. Signal Processing Algorithms. Prentice-Hall.
Truhar, N., Petrač, M., 2022. Damping optimization of linear vibrational systems with a singular mass matrix. Mathematics 10 (11), 1854.
Truhar, N., Tomljanovic, Z., Puvaca, M., 2017. An efficient approximation for optimal damping in mechanical systems. Int. J. Numer. Anal. Model. 14 (2), 201–217.
Truhar, N., Tomljanović, Z., Veselić, K., 2015. Damping optimization in mechanical systems with external force. Appl. Math. Comput. 250, 270–279.
Vasques, C.M.A., Moreira, R.A.S., Rodrigues, J.D., 2010a. Viscoelastic damping technologies - part I: modeling and finite element implementation. J. Adv. Res. Mech. Eng. 1 (2), 76–95.
Vasques, C.M.A., Moreira, R.A.S., Rodrigues, J.D., 2010b. Viscoelastic damping technologies - part II: experimental identification procedure and validation. J. Adv. Res. Mech. Eng. 1 (2), 96–110.
Venuti, F., Bruno, L., 2008. Pedestrian loads and dynamic performances of lively footbridges: an overview on measurement techniques and codes of practice. In: WIM (Weight In Motion), Load Capacity and Bridge Performance. 2nd Int. Workshop on Civil Struct. Health Monitoring, pp. 15–25.
Veselić, K., 2011. Damped Oscillations of Linear Systems: a Mathematical Introduction. Springer Sci. & Business Media Edition 2023.
Vinokur, R., 2003. The relationship between the resonant and natural frequency for non-viscous systems. J. Sound Vib. 267 (1), 187–189.
Wasmeier, P., 2003. The potential of object recognition using a servo-tacheometer TCA2003. Optical 3-D measurement techniques. VI(2), 48–54.
Webb, F.H. and Zumberge, J.F., 1996. An introduction to GIPSY/OASIS-II: precision software for the analysis of data from the Global Positioning System. Ed. JPL D-11088.
Woodhouse, J., 1998. Linear damping models for structural vibration. J. Sound Vib. 215 (3), 547–569.
Xu, P., Shi, C., Fang, R., et al., 2013. High-rate precise point positioning (PPP) to measure seismic wave motions: an experimental comparison of GPS PPP with inertial measurement units. J. Geod. 87 (4), 361–372.

Yi, T.H., Li, H.N., Gu, M., 2013. Experimental assessment of high-rate GPS receivers for deformation monitoring of bridge. Measurement 46 (1), 420–432.
Yoshida, J., Abe, M., Fujino, Y., Higashiuwatoko, K., 2002. Image analysis of human induced lateral vibration of a pedestrian bridge. In: Proceedings of the International Conference on the Design and Dynamic Behaviour of Footbridges, pp. 20–22.
Yu, J., Zhu, P., Xu, B., Meng, X., 2017. Experimental assessment of high sampling-rate robotic total station for monitoring bridge dynamic responses. Measurement 104, 60–69.
Zumberge, J., Heflin, M., Jefferson, D., Watkins, M., Webb, F., 1997. Precise point positioning for the efficient and robust analysis of GPS data from large networks. J. Geophys. Res. 102, 5005–5017.